

# Characterization of the pre-force-generation state in the actomyosin cross-bridge cycle

Mingxuan Sun<sup>†</sup>, Michael B. Rose<sup>†</sup>, Shobana K. Ananthanarayanan<sup>†</sup>, Donald J. Jacobs<sup>‡</sup>, and Christopher M. Yengo<sup>†§</sup>

Departments of <sup>†</sup>Biology and <sup>‡</sup>Physics and Optical Science, University of North Carolina, Charlotte, NC 28223

Edited by Thomas D. Pollard, Yale University, New Haven, CT, and approved April 1, 2008 (received for review November 14, 2007)

**Myosin is an actin-based motor protein that generates force by cycling between actin-attached (strong binding: ADP or rigor) and actin-detached (weak binding: ATP or ADP·P<sub>i</sub>) states during its ATPase cycle. However, it remains unclear what specific conformational changes in the actin binding site take place on binding to actin, and how these structural changes lead to product release and the production of force and motion. We studied the dynamics of the actin binding region of myosin V by using fluorescence resonance energy transfer (FRET) to monitor conformational changes in the upper-50-kDa domain of the actin binding cleft in the weak and strong actin binding states. Steady-state and lifetime data monitoring the FRET signal suggest that the cleft is in a more open conformation in the weak actin binding states. Transient kinetic experiments suggest that a rapid conformational change occurs, which is consistent with cleft closure before actin-activated phosphate release. Our results have identified a pre-force-generation actomyosin ADP·P<sub>i</sub> state, and suggest force generation may occur from a state not yet seen by crystallography in which the actin binding cleft and the nucleotide binding pocket are closed. Computational modeling uncovers dramatic changes in the rigidity of the upper-50-kDa domain in different nucleotide states, which suggests that the intrinsic flexibility of this domain allows myosin motors to accomplish simultaneous tight nucleotide binding (closed nucleotide binding pocket) and high-affinity actin binding (closed actin binding cleft).**

actin | energy transfer | motor proteins | myosin | structural dynamics

**A** current challenge in biophysics is to understand the mechanism of how motor proteins such as myosin convert chemical energy into mechanical work through a cyclic interaction with actin filaments. Numerous structure/function studies have converged on a structural model for force generation, where conformational changes in the active site are coupled to a large rotation of the light-chain binding region, also known as the lever arm hypothesis (1, 2). Myosin alters its affinity for actin in a nucleotide-dependent manner, from strong actin binding states (ADP or rigor state) to weak actin binding states (ATP or ADP·P<sub>i</sub> state), and thus phosphate release is believed to be associated with a large increase in actin affinity. Based on the high-resolution x-ray structure of myosin II (3) it was predicted that the actin binding cleft may open during ATP-induced dissociation of actomyosin and close during the release of the hydrolysis products induced by actin binding. The crystal structure of myosin V in the absence of nucleotide (rigor) demonstrated a closed conformation of the actin binding cleft (4, 5), and this structure fit quite well into the electron microscopy image reconstructions of the actomyosin rigor complex (6). Further studies of myosin II (7) and myosin V (8) by electron microscopy image reconstruction have demonstrated conformational changes in the actin binding cleft in different nucleotide states. Recently, the closed-cleft conformation was also observed in crystallographic studies of molluscan myosin II, wherein a “counterclockwise” orientation of the cleft rather than the extent of its closure was proposed to be critical for forming the strong binding rigor conformation (9).

By placing fluorescent probes in the actin binding cleft it was directly demonstrated that the cleft opens during ATP-induced dissociation of actomyosin (10, 11). However, there is currently no direct evidence that describes the kinetics of actin binding cleft closure in relationship to actin-activated phosphate release. In addition, there is a lack of information about how conformational changes in the cleft are coupled to structural changes in the nucleotide binding region. Most models of the actomyosin cross-bridge cycle suggest that myosin binds to actin through both ionic and hydrophobic interactions that stabilize a structural change in the actin binding region, such as closure of the actin binding cleft (1, 2). This structural change activates phosphate release through a series of conformational changes involving one or more of the elements of the active site that coordinate nucleotide binding: switch I, switch II, and the P loop. Finally, the swing of the lever arm and force generation is thought to occur before phosphate release (12–14). In the current study we demonstrate our ability to measure conformational changes in the actin binding region of myosin V associated with the transition from a weak to a strong actin binding complex and to correlate the kinetics of these conformational changes with biochemical steps in the actomyosin ATPase cycle.

In previous work, we labeled the upper-50-kDa domain of myosin V at residues 292–297 with the Fluorescein biArscenical Hairpin-binding dye (MV FIAsh) (15). Fluorescence resonance energy transfer (FRET) between mant-labeled nucleotides and MV FIAsh was used to demonstrate that the nucleotide binding pocket is more closed in the presence of ATP than ADP (1- to 2-Å distance change) in the absence of actin (15), which was also observed in other spectroscopic studies (16, 17). In addition, we found there was no change during the actin-activated phosphate release step, suggesting that force generation occurs from a state in which the nucleotide binding pocket remains closed. A possible explanation for these results is the existence of a unique conformational change in the upper-50-kDa domain in which the nucleotide binding pocket remains closed while the actin binding cleft closes down or rotates to allow strong actin binding. To test this possibility, we labeled actin at Cys-374 with IAEDANS (5((((2-iodoacetyl)amino)ethyl)amino)-naphthalene-1-sulfonic acid) (I-actin), and used the FRET between I-actin and MV FIAsh to study the structural dynamics of the upper-50-kDa domain during the actomyosin ATPase cycle. The FRET between these two probes allowed us to demonstrate a rapid temperature-dependent conformational change in myosin that occurs on binding to actin in the ADP·P<sub>i</sub> state. We conclude that a pre-force generation ADP·P<sub>i</sub> state is populated in the actomyosin ATPase cycle.

Author contributions: C.M.Y. designed research; M.S., M.B.R., S.K.A., D.J.J., and C.M.Y. performed research; D.J.J. and C.M.Y. contributed new reagents/analytic tools; M.S., M.B.R., D.J.J., and C.M.Y. analyzed data; and M.S., D.J.J., and C.M.Y. wrote the paper.

The authors declare no conflict of interest.

This article is a PNAS Direct Submission.

<sup>§</sup>To whom correspondence should be addressed. E-mail: cmyengo@uncc.edu.

This article contains supporting information online at [www.pnas.org/cgi/content/full/0710793105/DCSupplemental](http://www.pnas.org/cgi/content/full/0710793105/DCSupplemental).

© 2008 by The National Academy of Sciences of the USA

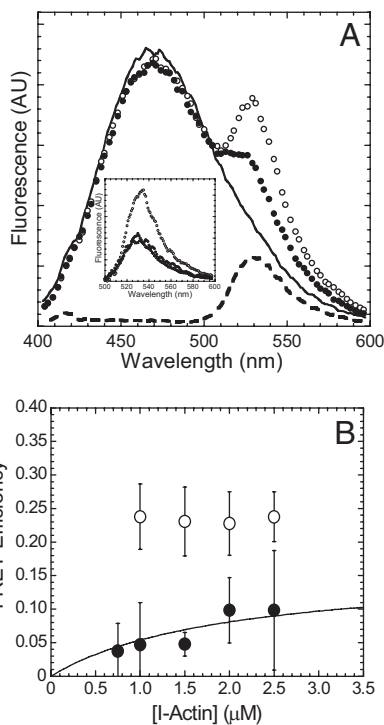


**Fig. 1.** Steady-state energy transfer of E442A MV FIAsh bound to I-actin. (A) The fluorescence spectra [arbitrary units (AU)] of I-actin ( $1 \mu\text{M}$ ) in the presence of unlabeled E442A MV ( $0.5 \mu\text{M}$ ) (black line), and E442A MV FIAsh in the absence (open circles) or presence of  $1 \text{ mM}$  ATP (filled circles). (Inset) The FIAsh fluorescence component of the spectra, corrected by subtracting the I-actin fluorescence component. The fluorescence spectrum of MV FIAsh alone is also shown (open triangles). (B) The FRET efficiency of E442A MV FIAsh in the absence (open circles) and presence of ATP (filled circles) were plotted as a function of I-actin concentration. The data in the presence of ATP are fit to a hyperbola to determine the efficiency extrapolated to 100% bound MV FIAsh. The error bars represent the S.D. from at least three separate experiments.

myosin ATPase cycle, which may be critical for the transition from weak to strong actin binding.

## Results

**IAEDANS-FIAsh FRET in the Weak and Strong Actin Binding States.** To investigate the weak binding states we generated myosin V with a point mutation in the switch II region (E442A MV) that essentially prevents ATP hydrolysis and therefore traps myosin

V in the prehydrolysis M-ATP state (18, 19). Wild-type myosin V (WT MV) was also used to examine the strong binding states and examine the transition from weak to strong binding in the transient kinetic experiments described below. The degree of energy transfer from I-actin to E442A MV FIAsh in the strong binding (nucleotide-free or rigor) and weak binding ( $1 \text{ mM}$  ATP) states was monitored by the enhancement of FIAsh fluorescence after subtraction of the contribution from I-actin fluorescence (Fig. 1). The efficiency of energy transfer ( $E$ ) with the I-actin ( $1 \mu\text{M}$ ) and MV FIAsh ( $0.5 \mu\text{M}$ ) pair in the rigor state was similar for WT and E442A MV FIAsh (data not shown). In the presence of ATP, the FRET efficiency was determined from the titration curve with I-actin, which allowed us to extrapolate the efficiency at 100% bound E442A MV FIAsh:I-actin ( $E_{\text{max}}$ ) (Fig. 1B) (15). The data were fit to a hyperbolic equation  $\{E = E_{\text{max}} * [\text{I-actin}] / (K_d + [\text{I-actin}])\}$ , where  $K_d = 2$  was determined from actin cosedimentation assays and a previous study (19). In the presence of ATP, the FRET efficiency was 7% lower for E442A MV FIAsh compared with rigor. The calculated distances ( $r$ ) between the FIAsh site and I-actin in the absence and presence of ATP are shown in Table 1.

The efficiency of energy transfer was also measured by examining the fluorescence lifetime of I-actin in the presence of both unlabeled and FIAsh labeled E442A MV (Fig. 2 and Table 1). Compared with the steady-state fluorescence results the energy transfer efficiency determined by monitoring the lifetime of the donor was found to be slightly higher in both the rigor ( $0.5 \mu\text{M}$  I-actin/ $1.0 \mu\text{M}$  E442A MV FIAsh) and ATP states ( $0.5 \mu\text{M}$  I-actin/ $2.8 \mu\text{M}$  MV FIAsh,  $1 \text{ mM}$  ATP) (Fig. 2, Table 1). The lifetime decays were best fit by a two-exponential function for the rigor complex and a three-exponential function in the presence of ATP (two bound components and one unbound component) (Fig. 2, supporting information (SI) Table S1). In the presence of ATP, the lifetime of the unbound component was similar to that of I-actin alone and the fractional amplitude of this component was similar that expected based on the affinity of E442A MV-ATP for I-actin.

**Transient Kinetic Measurements.** We examined the kinetics of the FRET signal with WT MV FIAsh binding to I-actin, or the pyrene signal with binding to pyrene actin in the strong binding rigor state (Fig. S1). The association rates of MV FIAsh binding to I-actin monitored by FRET were determined by examining the fluorescence increase in the acceptor (FIAsh) after mixing MV FIAsh ( $0.4 \mu\text{M}$  or  $0.8 \mu\text{M}$ ) with increasing concentrations of I-actin (5- to 10-fold excess I-actin) in the stopped flow. In the rigor state the fluorescence transients were fit to a single-

**Table 1. Summary of I-actin: MV FIAsh energy transfer results**

Nucleotide states	$R_0, \text{\AA}^*$	Steady state		Lifetime	
		FRET efficiency <sup>†</sup>	$r, \text{\AA}^\ddagger$ ( $r_{\text{min}}-r_{\text{max}}$ ) <sup>§</sup>	FRET efficiency <sup>¶</sup>	$r, \text{\AA}^\ddagger$ ( $r_{\text{min}}-r_{\text{max}}$ ) <sup>§</sup>
MV E442A FIAsh: I-actin (Rigor)	51	$0.23 \pm 0.02$	$62.4 \pm 1.2$ (43.4–81.9)	$0.36 \pm 0.05$	$56.1 \pm 2.2$ (40.0–73.7)
MV E442A FIAsh: I-actin (ATP)	51	$0.16 \pm 0.01$	$67.2 \pm 0.6$ (46.3–88.3)	$0.24 \pm 0.05$	$61.8 \pm 3.1$ (42.6–81.2)

\*Förster distance at which the efficiency of energy transfer is 50%.

<sup>†</sup>Steady-state FRET efficiency calculated from the titration curve with I-actin in the presence of ATP (errors represent standard error of the fit). In the rigor state errors represent standard deviation of the mean FRET efficiency.

<sup>‡</sup>Distance ( $r$ ) between the donor and acceptor probes calculated by using a  $\kappa^2$  value of 2/3.

<sup>§</sup>The range of distances ( $r_{\text{min}}-r_{\text{max}}$ ) possible based on the maximum and minimum value for  $\kappa^2$  determined from the steady-state and limiting anisotropy (20, 21).

<sup>¶</sup>FRET efficiency calculated from the decrease in donor lifetime ( $E = 1 - \tau_{\text{DA}}/\tau_{\text{D}}$ ). The average lifetime ( $\tau$ ) of the donor was determined in the presence and absence of acceptor. The errors represent the standard deviation of the mean from 3 to 4 separate experiments that included different protein preparations.

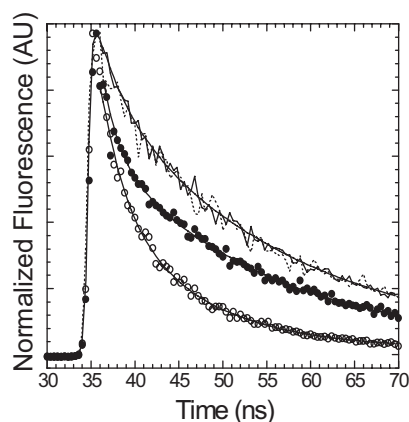


**Fig. 2.** Energy transfer between E442A MV FIAsh and I-actin examined by fluorescence lifetime measurements. Time-resolved fluorescence decays of 0.5  $\mu\text{M}$  I-actin were examined in the presence of 1.0  $\mu\text{M}$  unlabeled (dashed line) or FIAsh labeled (open circles) E442A MV in the rigor state and 2.8  $\mu\text{M}$  unlabeled (solid line) or FIAsh labeled (closed circles) E442A MV in the presence of 1 mM ATP. The data were fit to a two-exponential function in the rigor state and a three-exponential function in the presence of ATP. The average lifetime was calculated and used for the FRET efficiency measurements (see Table S1).

exponential function at each actin concentration measured. The donor-only control demonstrates that the I-actin fluorescence is minimal and does not change with unlabeled MV binding at the emission wavelengths examined (Fig. S1B). There was also no change in acceptor fluorescence associated with binding to unlabeled actin (Fig. S1B). The rates of binding to actin monitored by FRET were linearly dependent on actin concentration, which allowed us to determine the second-order rate constant associated with actin binding ( $39.1 \pm 2.1 \mu\text{M}^{-1} \text{s}^{-1}$ ) (Fig. S1A). The binding of MV FIAsh to pyrene actin was monitored by pyrene fluorescence quenching (Fig. S1A). In the absence of nucleotide, the fluorescence transients followed a single-exponential function, and the second-order binding constant determined from the linear fit of the binding rates was similar to the FRET signal ( $48.8 \pm 0.8 \mu\text{M}^{-1} \text{s}^{-1}$ ).

We examined the FRET signal during the weak-to-strong transition that occurs with MV FIAsh ADP-P<sub>i</sub> binding to I-actin. MV FIAsh (0.4–0.8  $\mu\text{M}$ ) was mixed with 20  $\mu\text{M}$  ATP, aged for 1 s, and then mixed with varying concentrations of I-actin (5- to 10-fold excess). The FIAsh fluorescence increase followed a biexponential function (Fig. 3). Both rates were linearly dependent on actin concentration and the amplitude was dominated by the fast phase, which had an actin dependence of  $49.0 \pm 3.0 \mu\text{M}^{-1} \text{s}^{-1}$ . The slow phase ( $4.7 \pm 0.3 \mu\text{M}^{-1} \text{s}^{-1}$ ) was <20% of the total amplitude and the relative amplitudes were similar at each actin concentration measured. The donor-only control demonstrates no change with unlabeled MV binding to I-actin in ADP-P<sub>i</sub> state. However, the acceptor-alone control shows a small rise (actin dependence  $\approx 5 \mu\text{M}^{-1} \text{s}^{-1}$ ) on mixing of MV FIAsh with unlabeled actin in the ADP-P<sub>i</sub> state, which is similar to the slow phase in the FRET signal.

For comparison to our FRET signal, actin-activated phosphate release was measured. We examined the rate of actin-activated phosphate release by using a sequential-mix experiment identical to that described above, but with the phosphate-binding protein (PBP) in the final mix (Fig. 3A). The PBP fluorescence increase was fit to a burst followed by a linear phase. The burst rate was plotted as a function of I-actin concentration, and a linear fit was used to determine the second-order rate constant for actin-activated phosphate release ( $9.6 \pm 0.4 \mu\text{M}^{-1} \text{s}^{-1}$ ).

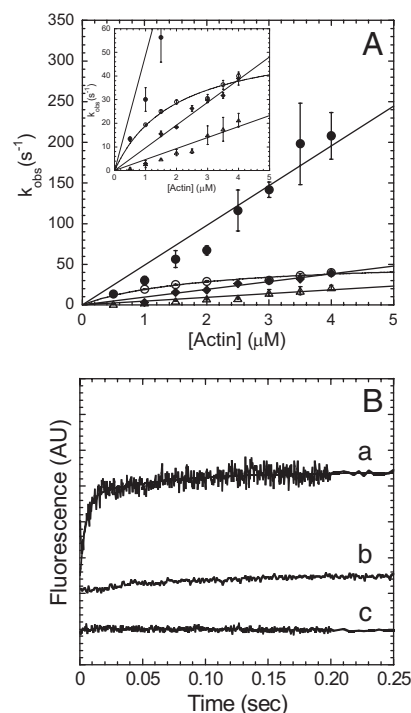


**Fig. 3.** MV FIAsh binding to actin in the ADP-P<sub>i</sub> state. The kinetics of the FRET signal was compared with the pyrene actin and phosphate release signals. (A) The FRET signal measured on MV FIAsh ADP-P<sub>i</sub> binding to I-actin monitored by the increase in FIAsh fluorescence was fit to a biexponential function at each I-actin concentration. The fast rate (filled circles) and the slow rate (open triangles) were linearly dependent on I-actin concentration. MV FIAsh ADP-P<sub>i</sub> binding to pyrene actin was hyperbolically dependent on actin concentration (open circles). The phosphate release rate was linearly dependent on I-actin concentration (filled diamonds). (Inset) Close-up of the phosphate release and pyrene actin plots. (B) Fluorescence traces of the FRET signal (a) monitored by the enhancement of FIAsh fluorescence and fit to a two-exponential function (final conditions: 0.2  $\mu\text{M}$  MV FIAsh, 10  $\mu\text{M}$  ATP, 2  $\mu\text{M}$  I-actin;  $k_{\text{obs}} = 143 \pm 17$  and  $12 \pm 2 \text{ s}^{-1}$ ), compared with the donor-alone (b) (final conditions: 0.2  $\mu\text{M}$  unlabeled MV, 10  $\mu\text{M}$  ATP, and 2  $\mu\text{M}$  I-actin) and acceptor-alone (c) (final conditions: 0.2  $\mu\text{M}$  MV FIAsh, 10  $\mu\text{M}$  ATP, 2  $\mu\text{M}$  unlabeled actin).

To compare our FRET signal with the pyrene actin signal, a sequential mix experiment was also performed to monitor MV ADP-P<sub>i</sub> binding to pyrene actin (Fig. 3A). Using the experimental design described above we found the rates of pyrene fluorescence quenching followed a single exponential function. The rate of the pyrene fluorescence decrease was plotted as a function of pyrene actin concentration and fit to a hyperbola with a maximum binding rate of  $56.4 \pm 6.9 \text{ s}^{-1}$ . The linear phase of the curve demonstrated a second-order binding constant of  $28.6 \pm 4.8 \mu\text{M}^{-1} \text{s}^{-1}$ .

The temperature dependence of the FRET signal observed with MV FIAsh ADP-P<sub>i</sub> binding to I-actin was determined by performing the sequential-mix experiments described above at 15°C (Fig. 4). At 15°C, the rate of the MV FIAsh fluorescence enhancement was fit to a single-exponential function at each I-actin concentration. The second-order rate constant calculated from the linear fit of the FRET transients was  $15.5 \pm 1.3 \mu\text{M}^{-1} \text{s}^{-1}$  at 15°C, which is  $\approx 3$ -fold slower than that measured at 25°C.

## Discussion

Our data provide critical information about the conformational changes in myosin that are associated with the transition from weak to strong actin binding. The FRET efficiency with the I-actin: MV FIAsh pair is  $\approx 7\%$  reduced in the weak binding states compared with the strong binding rigor state in the



phate release has been intensely examined with intact muscle fiber studies (12–14, 26, 27), solution biochemistry experiments with purified proteins (28–30), and single-molecule studies (31, 32). Currently the most widely accepted model suggests that myosin in the  $M \cdot ADP \cdot P_i$  state binds weakly to actin, undergoes a weak-to-strong transition forming a strongly bound actomyosin complex, which is followed by force generation and phosphate release (12–14). Key results from optical trap studies, and tension-recovery modeling on the timing of phosphate release in skeletal muscle myosin demonstrate that force generation occurs before  $P_i$  release (12–14). In this study, we observed a new  $AM \cdot ADP \cdot P_i$  intermediate during the actomyosin ATPase cycle. This intermediate is associated with a fast conformational change on  $MV \cdot ADP \cdot P_i$  binding to actin and may allow for rapid attachment to actin before force generation.

If the conformational change monitored by FRET is closure of the actin binding cleft, myosin must close down the cleft immediately on  $M \cdot ADP \cdot P_i$  binding to actin ( $k'_{+4A}$ ), and adopt a strongly bound conformation in the  $AM' \cdot ADP \cdot P_i$  state. Our results suggest that  $M \cdot ADP \cdot P_i$  binds to actin, followed by a fast rotation of the upper-50-kDa domain that results in closure of the actin binding cleft. This conformational change may cause distortion of the transducer region ( $\beta$ -sheet), generating strain-dependent tension that subsequently results in actin-activated phosphate release through the “back door” (33). A strongly bound  $AM \cdot ADP \cdot P_i$  state has been proposed based on muscle fiber studies (14), single-molecule laser trap studies (32), and rapid freezing EM studies (34). The large temperature dependence of the conformational change ( $Q_{10} = 3.2$ ) is consistent with a significant domain motion such as cleft closure that proceeds through a large activation energy barrier ( $U_a \approx 34 k_B T$ ). Structural and biochemical analysis of the nucleotide-free state in different myosin isoforms demonstrates that temperature-dependent rigor binding is an indication that cleft closure occurs during the binding process (i.e., a large temperature dependence for skeletal muscle myosin,  $U_a \approx 28 k_B T$ , and little or no temperature dependence for myosin V) (4, 9, 23). Thus, our temperature-dependent results are consistent with previous reports describing the energetics of cleft closure.

**Structural Rearrangement of Loop 2.** Alternatively, the fast conformational change monitored by our FRET signal could be a conformational change in some other element of the actin binding region, such as within loop 2. A cryo-EM study suggests that loop 2 may adopt different conformations in different nucleotide states ( $AM \cdot ADP$ /rigor,  $AM \cdot ADP \cdot P_i$ , and  $AM \cdot ATP$ ), and might be important for allowing myosin to stay loosely attached to actin in the weak binding states (8). If our data represent a conformational change in loop 2, this would suggest that there is a fast structural rearrangement in loop 2 during the weak-to-strong transition. Our results may fit in with the cryo-EM studies, which suggest that loop 2 adopts a more ordered conformation in the strongly bound state (rigor, ADP). These studies suggest that loop 2 rearranges in the ATP state, and rearranges again in the transition state ( $M \cdot ADP \cdot P_i$ ). If the structural rearrangement of loop 2 is the fast conformational change we observed by our FRET signal, myosin must undergo another conformational change to close down the actin binding cleft. Because we did not observe a second slower transition in our FRET signal we feel that this interpretation is not likely. However, it is possible that the cleft closes by a unique rotation of the upper-50-kDa domain that does not change the distance between our  $MV$  FAsH/I-actin donor/acceptor pair.

**Dynamics of the Upper-50-kDa Domain in Myosin.** The recent rigor structures of molluscan myosins demonstrated that different conformations of the “inner” and “outer” actin binding cleft are possible (9), which implies that the cleft has some intrinsic

flexibility. We investigated the possibility that a change in the flexibility of the upper-50-kDa domain allows myosin to adopt a closed nucleotide binding pocket and closed actin binding cleft conformation. We examined the RMSD of alpha carbon atoms in the myosin V rigor, ADP, and  $ADP \cdot BeF_x$  crystal structures (4, 5) by performing geometric simulations (35, 36) (see supplemental data in Figs. S2 and S3). We find that the upper-50-kDa domain is more flexible in the ADP state than in the  $ADP \cdot BeF_x$  and rigor states. These results show that the intrinsic flexibility of the upper-50-kDa domain may play a role in allowing myosin to rapidly adopt the strongly bound pre-force conformation. Interestingly, the increased flexibility of the upper-50-kDa domain in the ADP state may allow myosin motors to simultaneously bind tightly to actin and ADP. Because there is a large amount of variability within the myosin superfamily in the degree of coupling between the nucleotide and actin binding regions, the flexibility of the upper-50-kDa domain may be an important determinant of degree of nucleotide/actin coupling in myosin motors.

In conclusion, we observed a pre-force generation actomyosin  $ADP \cdot P_i$  intermediate during the myosin cross-bridge cycle by monitoring the FRET signal between I-actin and  $MV$  FAsH. We demonstrate a temperature-dependent conformational change before phosphate release associated with  $M \cdot ADP \cdot P_i$  binding to actin, which may be important for rapid attachment to actin before phosphate release and force generation. Our results suggest that force generation occurs in a structural state of myosin not yet seen by crystallographic studies, which has both a closed actin binding cleft and closed nucleotide binding pocket.

## Materials and Methods

**Myosin V cDNA Construction, Expression, and Purification.** Myosin V 11Q constructs (wild-type and E442A  $MV$ ) containing the upper-50-kDa tetracycline motif, were coexpressed with calmodulin by using the baculovirus system (15). FAsH labeling was very efficient ( $\geq 95\%$ ) as determined by absorbance measurements (15). Actin was purified from rabbit skeletal muscle by using an acetone powder method (37) and labeled with pyrene iodoacetamide (38) or 5((((2-iodoacetyl) amino) ethyl) amino)-naphthalene-1-sulfonic acid (IAEDANS) (39). All experiments were performed in  $KMg50$  TCEP buffer (50 mM KCl, 1 mM EGTA, 1 mM  $MgCl_2$ , 1 mM TCEP, and 10 mM imidazole-HCl, pH 7.0).

**FRET Measurements.** A Quantamaster fluorometer (Photon Technology International), equipped with a 75-watt xenon arc lamp as an excitation source and excitation/emission monochromators, was used to measure steady-state fluorescence. Steady-state energy transfer measurements were performed by exciting I-actin at 365 nm, and the emission was measured from 400 to 600 nm with a 0.5-nm band pass. The enhancement in acceptor fluorescence was used to calculate the energy transfer efficiency after subtraction of the donor fluorescence (15, 21, 40). Fluorescence lifetime experiments were performed with a Timemaster Fluorescence Spectrometer (PTI), equipped with a picosecond pulse  $N_2$  dye laser. I-actin fluorescence was excited at 366 nm with a  $N_2$  dye laser and the emission measured through a single-grating monochromator at 471 nm. Fluorescence decays were analyzed with Global analysis software provided with the instrument. The quantum yield ( $Q_D$ ) of the donor, extinction coefficients of the donor ( $\epsilon_D$ ) and acceptor ( $\epsilon_A$ ) at the donor excitation wavelength (365 nm), and overlap integral for the I-actin: $MV$  FAsH pair [ $J(\lambda)$ ] were,  $Q_D = 0.38$  (<5% change was observed in the ATP and rigor states),  $\epsilon_A = 1,259 M^{-1} cm^{-1}$  (15),  $\epsilon_D = 5,700 M^{-1} cm^{-1}$  (39),  $J(\lambda) = 3.2 \times 10^{-13} cm^3 M^{-1}$  and used in our FRET calculations. The steady-state ( $r$ ) (measured in  $KMg50$  at 25°C) and limiting ( $r_0$ ) anisotropy (measured in  $KMg50$  in a glycerol solution at -14°C) was measured for the donor and acceptor fluorophore in the rigor and ATP states (see Table S2).

**Kinetic Measurements.** Transient kinetic experiments were performed in an Applied Photophysics stopped-flow apparatus with a dead time of 1.2 ms. Pyrene actin was excited at 365 nm, and the fluorescence emission was measured by using a 400-nm long pass filter. FAsH fluorescence was measured by energy transfer from I-actin by exciting at 365 nm and the emission was measured with a 515-nm long pass filter. Nonlinear least-squares fitting of the data was done with software provided with the instrument or Kaleidagraph (Synergy Software). Phosphate release experiments were performed by exciting the PBP at 400 nm and measuring the emission with a 420-nm long pass

filter (22). Uncertainties reported are standard error of the fits unless stated otherwise. Kinetic modeling and simulations were performed with Pro-K software (Applied Photophysics) using a standard myosin V reaction scheme (15, 22–25) or Scheme 1. All concentrations mentioned in the stopped-flow experiments are final concentrations unless stated otherwise.

**Computational Modeling.** Three x-ray crystal structures from the Protein Data Bank (PDB ID codes 1OE9, 1W7J, and 1W7I) were used respectively to represent the Rigor, ADP.BeFx, and ADP conformational states of myosin V. Floppy Inclusions and Rigid Substructure Topography [FIRST (35)] was used to determine the number of independent degrees of freedom and identify flexible and rigid regions within each structure. We used the Framework Rigidity

Optimized Dynamic Algorithm (FRODA) to perform a geometric simulation (36). The root-mean-square displacement (rmsd) for carbon-alpha atoms was calculated for each structure (see Fig. S2 for detailed methods).

**ACKNOWLEDGMENTS.** We thank Dr. Howard White for the phosphate-binding protein, Andrei Istomin for the homology modeling on myosin V to incorporate loop 2 into the structure, Dorit Hanein and Niels Volkman for sharing the coordinates for the myosin V cryo-EM structures and Stephen Adams and Roger Tsieu for providing FIAsH. This work was supported in part by an American Heart Association Scientist Development Grant (to C.M.Y.), National Institutes of Health R01 GM073082-01A1 (to D.J.J.), the Center for Biomedical Engineering Systems, and the UNC Charlotte Graduate School.

- Holmes KC, Geeves MA (1999) Structural mechanism of muscle contraction. *Annu Rev Biochem* 68:687–728.
- Sweeney HL, Houdusse A (2004) The motor mechanism of myosin V: Insights for muscle contraction. *Philos Trans R Soc B* 359:1829–1841.
- Rayment I, et al. (1993) Three-dimensional structure of myosin subfragment-1: A molecular motor. *Science* 261:50–58.
- Coureux P, et al. (2003) A structural state of the myosin V motor without bound nucleotide. *Nature* 425:419–423.
- Coureux P, Sweeney HL, Houdusse A (2004) Three myosin V structures delineate essential features of chemo-mechanical transduction. *EMBO J* 23:4527–4537.
- Holmes KC, Schroder RR, Sweeney HL, Houdusse A (2004) The structure of the rigor complex and its implications for the power stroke. *Philos Trans R Soc Lond B Biol Sci* 359:1819–1828.
- Volkman N, et al. (2000) Evidence for cleft closure in actomyosin upon ADP release. *Nat Struct Biol* 7:1147–1155.
- Volkman N, et al. (2005) The structural basis of myosin V processive movement as revealed by electron cryomicroscopy. *Mol Cell* 19:595–605.
- Yang Y, et al. (2007) Rigor-like structures from muscle myosins reveal key mechanical elements in the transduction pathways of this allosteric motor. *Structure* 15:553–564.
- Yengo CM, De La Cruz EM, Chrin LR, Gaffney II DP, Berger CL (2002) Actin-induced closure of the actin-binding cleft of smooth muscle myosin. *J Biol Chem* 277:24114–24119.
- Conibear PB, Bagshaw CR, Fajer PG, Kovacs M, Malnasi-Csizmadia A (2003) Myosin cleft movement and its coupling to actomyosin dissociation. *Nat Struct Biol* 10:831–835.
- Dantzig JA, Goldman YE, Millar NC, Laktick J, Homsher E (1992) Reversal of the cross-bridge force-generating transition by photogeneration of phosphate in rabbit psoas muscle fibers. *J Physiol* 451:247–278.
- Smith DA, Sleep J (2004) Mechanokinetics of rapid tension recovery in muscle: The myosin working stroke is followed by a slower release of phosphate. *Biophys J* 87:442–456.
- Takagi Y, Shuman H, Goldman YE (2004) Coupling between phosphate release and force generation in muscle actomyosin. *Philos Trans R Soc Lond B Biol Sci* 359:1913–1920.
- Sun M, et al. (2006) Dynamics of the upper 50 kDa domain of myosin V examined with fluorescence resonance energy transfer. *J Biol Chem* 281:5711–5717.
- Robertson I, Gaffney DP, Chrin LR, Berger CL (2005) Structural rearrangements in the active site of smooth-muscle myosin. *Biophys J* 89:1882–1892.
- Naber N, Purcell TJ, Pate E, Cooke R (2007) Dynamics of the nucleotide pocket of myosin measured with spin-labeled nucleotides. *Biophys J* 92:172–184.
- Sasaki N, Shimada T, Sutoh K (1998) Mutational analysis of the switch II loop of Dictyostelium myosin II. *J Biol Chem* 273:20334–20340.
- Yengo CM, De La Cruz EM, Safer D, Ostap EM, Sweeney HL (2002) Kinetic characterization of the weak binding states of myosin V. *Biochemistry* 41:8508–8517.
- Dale RE, Eisinger J (1974) Intramolecular distances determined by energy transfer: Dependence on orientational freedom of donor and acceptor. *Biopolymers* 13:1573–1605.
- Lakowicz JR (2006) *Principles of Fluorescence Spectroscopy* (Springer, New York, NY), 3rd Ed.
- Yengo CM, Sweeney HL (2004) Functional role of loop 2 in myosin V. *Biochemistry* 43:2605–2612.
- De La Cruz EM, Wells AL, Rosenfeld SS, Ostap EM, Sweeney HL (1999) The kinetic mechanism of myosin V. *Proc Natl Acad Sci USA* 96:13726–13731.
- Rosenfeld SS, Sweeney HL (2004) A model of myosin V processivity. *J Biol Chem* 279:40100–40111.
- Hannemann DE, Cao W, Olivares AO, Robblee JP, De La Cruz EM (2005) Magnesium, ADP, and actin binding linkage of myosin V: Evidence for multiple myosin V-ADP and actomyosin V-ADP states. *Biochemistry* 44:8826–8840.
- Hibberd MG, Dantzig JA, Trentham DR, Goldman YE (1985) Phosphate release and force generation in skeletal muscle fibers. *Science* 228:1317–1319.
- Hibberd MG, Webb MR, Goldman YE, Trentham DR (1985) Oxygen exchange between phosphate and water accompanies calcium-regulated ATPase activity of skinned fibers from rabbit skeletal muscle. *J Biol Chem* 260:3496–3500.
- Lynn RW, Taylor EW (1971) Mechanism of adenosine triphosphate hydrolysis by actomyosin. *Biochemistry* 10:4617–4624.
- White HD, Taylor EW (1976) Energetics and mechanism of actomyosin adenosine triphosphatase. *Biochemistry* 15:5818–5826.
- White HD, Belknap B, Webb MR (1997) Kinetics of nucleoside triphosphate cleavage and phosphate release steps by associated rabbit skeletal actomyosin, measured using a novel fluorescent probe for phosphate. *Biochemistry* 36:11828–11836.
- Takagi Y, Homsher EE, Goldman YE, Shuman H (2006) Force generation in single conventional actomyosin complexes under high dynamic load. *Biophys J* 90:1295–1307.
- Baker JE, Brosseau C, Joel PB, Warshaw DM (2002) The biochemical kinetics underlying actin movement generated by one and many skeletal muscle myosin molecules. *Biophys J* 82:2134–2147.
- Lawson JD, Pate E, Rayment I, Yount RG (2004) Molecular dynamics analysis of structural factors influencing back door pi release in myosin. *Biophys J* 86:3794–3803.
- Walker M, Zhang XZ, Jiang W, Trinick J, White HD (1999) Observation of transient disorder during myosin subfragment-1 binding to actin by stopped-flow fluorescence and millisecond time resolution electron cryomicroscopy: Evidence that the start of the crossbridge power stroke in muscle has variable geometry. *Proc Natl Acad Sci USA* 95:8034–8039.
- Jacobs DJ, Rader A, Kuhn LA, Thorpe MF (2001) Protein flexibility predictions using graph theory. *Proteins* 44:150–165.
- Wells S, Menor S, Hespeneide B, Thorpe MF (2005) Constrained geometric simulation of diffusive motion in proteins. *Phys Biol* 2:S127–S136.
- Pardee JD, Spudich JA (1982) Purification of muscle actin. *Methods Enzymol* 85:164–181.
- Pollard TD (1984) Polymerization of ADP-actin. *J Cell Biol* 99:769–777.
- Yengo CM, Chrin LR, Berger CL (2000) Interaction of myosin LYS-553 with the C-terminus and DNase I-binding loop of actin examined by fluorescence resonance energy transfer. *J Struct Biol* 131:187–196.
- Clegg RM (1992) Fluorescence resonance energy transfer and nucleic acids. *Methods Enzymol* 211:353–388.